NeuroImage: Clinical 17 (2018) 751–760

Contents lists available at ScienceDirect

NeuroImage: Clinical

journal homepage: www.elsevier.com/locate/ynicl

# Regional association of pCASL-MRI with FDG-PET and PiB-PET in people at risk for autosomal dominant Alzheimer's disease

Lirong Yan[a,b,*], Collin Y. Liu[b,c], Koon-Pong Wong[d], Sung-Cheng Huang[d], Wendy J. Mack[e], Kay Jann[a,b], Giovanni Coppola[f], John M. Ringman[b,c], Danny J.J. Wang[a,b]

[a] Laboratory of FMRI Technology (LOFT), USC Stevens Neuroimaging and Informatics Institute, Keck School of Medicine, University of Southern California, Los Angeles, CA, USA
[b] Department of Neurology, University of Southern California, Los Angeles, CA, USA
[c] Alzheimer's Disease Research Center, University of Southern California, Los Angeles, CA, USA
[d] Molecular and Medical Pharmacology, University of California Los Angeles, Los Angeles, CA, USA
[e] Department of Preventive Medicine, Keck School of Medicine, University of Southern California, Los Angeles, CA, USA
[f] Semel Institute of Psychiatry and Biobehavioral Sciences UCLA, USA

ARTICLE INFO

*Keywords:*
Autosomal dominant Alzheimer's disease
Arterial spin labeling
MRI
FDG pet
PiB PET
Cerebral perfusion
Glucose metabolism
Amyloid deposition

ABSTRACT

Autosomal dominant Alzheimer's disease (ADAD) is a small subset of Alzheimer's disease that is genetically determined with 100% penetrance. It provides a valuable window into studying the course of pathologic processes that leads to dementia. Arterial spin labeling (ASL) MRI is a potential AD imaging marker that non-invasively measures cerebral perfusion. In this study, we investigated the relationship of cerebral blood flow measured by pseudo-continuous ASL (pCASL) MRI with measures of cerebral metabolism (FDG PET) and amyloid deposition (Pittsburgh Compound B (PiB) PET). Thirty-one participants at risk for ADAD (age 39 ± 13 years, 19 females) were recruited into this study, and 21 of them received both MRI and FDG and PiB PET scans. Considerable variability was observed in regional correlations between ASL-CBF and FDG across subjects. Both regional hypo-perfusion and hypo-metabolism were associated with amyloid deposition. Cross-sectional analyses of each biomarker as a function of the estimated years to expected dementia diagnosis indicated an inverse relationship of both perfusion and glucose metabolism with amyloid deposition during AD development. These findings indicate that neurovascular dysfunction is associated with amyloid pathology, and also indicate that ASL CBF may serve as a sensitive early biomarker for AD. The direct comparison among the three biomarkers provides complementary information for understanding the pathophysiological process of AD.

## 1. Introduction

Alzheimer's disease (AD), as the most common form of dementia, is one of the leading causes of death in the United States. Converging evidence indicates that AD pathology begins years or decades before the clinical symptoms appear (Bateman et al., 2012; Dubois et al., 2016; Frisoni, 2012). Longitudinal studies of AD biomarkers therefore take many years to capture the full pathologic processes leading to dementia. Fully-penetrant autosomal dominant AD (ADAD) due to *PSEN1*, *PSEN2*, or *APP* mutations provides a valuable window for studying biomarkers across the cascade of AD pathology by taking advantage of the essentially 100% penetrance for the future development of AD with similar age of onset within families and mutation type (Ryman et al., 2014; Bateman et al., 2011; Schindler & Fagan, 2015). Therefore, we can estimate at what point cognitive, behavioral, imaging, and biochemical changes are occurring with respect to the onset of clinical signs. At least some findings in this population will likely be applicable to late-onset AD (LOAD) as ADAD and LOAD have similar, though not identical, clinical features, amyloid plaque and neurofibrillary tangle pathology, and early cerebrospinal fluid changes (Bateman et al., 2012).

Over the past decade, various imaging modalities including positron emission tomography (PET) and magnetic resonance imaging (MRI) have been investigated as surrogate biomarkers of AD (S Zhang et al., 2014a; Vlassenko et al., 2012; Ewers et al., 2011; Mosconi et al., 2010; Smailagic et al., 2015; Fennema-Notestine et al., 2009; Frisoni et al., 2010; Berti et al., 2010). Brain atrophy (Frisoni et al., 2010; McDonald et al., 2009; Vemuri, 2010), cerebral perfusion (Binnewijzend et al.,

* Corresponding author at: Laboratory of FMRI Technology (LOFT), USC Stevens Neuroimaging and Informatics Institute, Department of Neurology, Keck School of Medicine, University of Southern California, 2025 Zonal Ave, Los Angeles, CA, 90033, USA.
*E-mail address:* lyan@ini.usc.edu (L. Yan).

https://doi.org/10.1016/j.nicl.2017.12.003
Received 28 June 2017; Received in revised form 27 November 2017; Accepted 2 December 2017
Available online 06 December 2017

2013; Binnewijzend et al., 2016), metabolism (Mosconi et al., 2010; Mosconi, 2005), and amyloid and Tau deposition (Forsberg et al., 2008; Small et al., 2006) have been extensively quantified. $^{18}$F-FDG PET is used to assess the neurodegenerative processes in AD by measuring glucose metabolism (Smailagic et al., 2015; Mosconi, 2005). Reduction of regional cerebral metabolism has been well characterized in AD patients, and even in MCI patients (Alexander et al., 2002; Mosconi et al., 2009). Many studies suggest cerebral metabolic changes measured using FDG PET can occur as early as the third decade of life (Reiman et al., 2004; Loessner et al., 1995). [$^{11}$*C*]Pittsburgh compound B ([$^{11}$*C*]PiB) PET amyloid imaging (Klunk et al., 2004) has been widely used since the accumulation of amyloid β plaques in the brain is thought to play a causative role in AD based on the amyloid cascade hypothesis (Hardy & Higgins, 1992). Specifically, the tracer kinetic modeling of PiB PET yields multiple parameters, including the distribution volume ratio (DVR) of PiB, which is used for the assessment of amyloid deposition, and R1, which is related to tracer delivery, providing information on regional perfusion (Lammertsma & Hume, 1996; Logan, 2000).

While the presence of amyloid plaques is recognized as a central event in the pathogenesis of AD, there is growing evidence that vascular factors play an important role as well (Dickstein et al., 2010; Murray et al., 2011). Decreased regional cerebral blood flow (CBF) has been extensively studied as a possible biomarker of AD (Hays et al., 2016). Arterial spin labeling (ASL) provides a noninvasive means of quantifying regional CBF by MRI, which utilizes magnetically labeled arterial blood water as an endogenous tracer (Detre et al., 2009). Compared to $^{15}$O-water PET perfusion imaging, ASL does not involve radiation or contrast injection, and provides absolute CBF measurement and allows easy registration with structural MRI. Over the past few years, several groups have successfully applied ASL MRI to AD (Alsop et al., 2010; Z Wang et al., 2013a; Alsop et al., 2000; Johnson et al., 2005; Dai et al., 2009; WT et al., 2010). Characteristic patterns of cerebral hypoperfusion were detected using ASL MRI, mostly in late-onset AD patients (Alsop et al., 2010; Z Wang et al., 2013a; Alsop et al., 2000; Johnson et al., 2005; Dai et al., 2009; WT et al., 2010). A good correlation has been demonstrated between ASL MRI and $^{15}$O-water PET in both resting state and activation studies (Ye et al., 2000; K Zhang et al., 2014b; Kilroy et al., 2014). More recently, a few groups began to investigate the relationship between cerebral perfusion by ASL MRI and metabolism by FDG PET (Cha et al., 2013; Chen et al., 2011), as well as between ASL MRI and PiB PET (McDade et al., 2014; Mattsson et al., 2014). However, we are unaware of any studies that have directly compared CBF measured by ASL MRI with both metabolism and amyloid deposition measured by PET in persons at risk for ADAD. Therefore, the aim of this study was to enhance our understanding of the contributions of both vascular, metabolic and biochemical dysfunction to the amyloid pathology of AD by investigating the relationship among cerebral perfusion, glucose metabolism, and amyloid deposition in a cohort of individuals at risk for ADAD.

## 2. Materials and methods

### 2.1. Study participants

Persons known to have *PSEN1*, *PSEN2*, or *APP* mutations in the family were recruited for comprehensive clinical, imaging, and biochemical assessments at UCLA. A total of 31 ADAD subjects (age 39 ± 13 years, 19 females) including 23 mutation carriers (PSEN = 19, and APP = 4) participated in this study after providing written informed consent. Persons with significant medical or psychiatric illnesses with the potential to significantly affect their cognition were excluded.

### 2.2. MRI protocol

Twenty-seven participants underwent MRI scans on a 3 T Siemens TIM Trio scanner (Erlangen, Germany) using the standard 12-channel head coil. Two participants were excluded from data analysis due to abnormal CBF values of whole brain (e.g. < 20 ml/100 g/min). Pseudo-continuous ASL (pCASL) with 3D background suppressed GRASE sequence (Kilroy et al., 2014) was performed for resting CBF measurement with the following imaging parameters: FOV = 220 × 220 mm$^2$, matrix size = 64 × 64, TE/TR = 23/3500 ms, GRAPPA rate = 2. Twenty-six 5-mm slices were acquired to cover the whole brain with 60 repetitions. The tagging plane was positioned 90 mm inferior to the center of the imaging slab with a labeling duration of 1500 ms and post-labeling delay (PLD) of 1500 ms. A 3D MPRAGE sequence was performed for T1 weighted structural MRI with the imaging parameters: 192 slices at 1 mm slice thickness, voxel size = 1 × 1 × 1 mm$^3$, TR/TE = 1620/3 ms, TI = 950 ms, TE = 3 ms, the scan time of 6 min.

### 2.3. PET protocol

#### 2.3.1. $^{18}$F-FDG PET

Twenty-three subjects participated in an $^{18}$F-FDG PET/CT scan on a whole body scanner. Metabolic imaging with [18*F*]FDG-PET was performed with a 3D dynamic acquisition beginning 40 min after a bolus injection of approximately 5 mCi of FDG and lasted for 20 min. Images were reconstructed using back of projection with a Gaussian smoothing of 3 mm full width half-maximum (FWHM) after correction for scatter, decay, scanner dead time, and attenuation.

#### 2.3.2. $^{11}$C-PiB PET

Twenty-three participants received $^{11}$C-PIB PET/CT scans. Subjects received a bolus injection of approximately 15 mCi of [11*C*]PiB. Dynamic $^{11}$C-PIB PET/CT scans were acquired in list-mode for 70 min. Raw PiB PET data were rebinned into 6 × 30 s, 4 × 180 s, and 11 × 300 s, and were reconstructed using ordered subset expectation maximization algorithm (6 iterations, 16 subsets) with a post-reconstruction 3D Gaussian smoothing (FWHM: 3 mm × 3 mm × 3 mm). A retrospective image-based movement correction procedure was applied to correct for possible misalignment between CT and PET scans and between PET image frames (Ye et al., 2014).

### 2.4. Image processing

For pCASL data, motion correction was performed using Statistical Parametric Mapping (SPM) 12 for control and label images, separately. Perfusion weighed images were obtained by pair-wise subtraction between the control and label images. Quantitative CBF maps were subsequently calculated using the averaged perfusion weighted images based on a single compartment model (Kilroy et al., 2014).

All CBF, FDG PET, and PiB PET images of each subject were co-registered to the subject's MPRAGE images, and further warped to MNI single-subject brain template using the Symmetric Diffeomorphic Mapping method implemented in ANTS (Avants et al., 2008). The normalized CBF images were smoothed with a 3 mm FWHM kernel, creating absolute CBF (absCBF) maps. A relative CBF (rCBF) map was also generated by dividing the CBF of each voxel by the mean CBF in the cerebellum for each subject. Summation images were generated from FDG PET data to assess the glucose metabolism, and then were intensity normalized to cerebellar mean intensity, generating relative $CMR_{Glc}$ ($rCMR_{Glc}$) images. For PiB PET images, using the combined transformation from template to PET space, tissue time-activity curve was generated for cerebellar grey matter (reference region), and parametric images of relative perfusion (R1) and distribution volume ratio (DVR) were constructed by simplified reference tissue model (SRTM) (Lammertsma & Hume, 1996) and Logan graphical method (Logan,

2000), respectively.

For each subject, normalized MPRAGE images were segmented into grey matter (GM), white matter (WM) and cerebrospinal fluid (CSF) compartment using SPM 12. A grey matter mask thresholded for probabilities above 90% from the GM segmentation was applied for CBF, $rCMR_{Glu}$, DVR and R1 images before performing regional correlation analysis. To specify regional correlations, the CBF, $rCMR_{Glu}$, DVR and R1 images were compared within 9 representative of regions of interest (ROIs) from the Anatomic Labeling (AAL) template in SPM including the frontal, parietal, occipital, and temporal lobes, amygdala, caudate, cingulum, hippocampus, and insula. Cross-sectional analyses of the mean CBF, $rCMR_{Glu}$, and DVR of each ROI were performed as a function of the parental age at onset. Jacobian determinants were also calculated from the T1 structural images of each participant, which were used for correction of expansion or contraction of a voxel during spatial normalization (Du et al., 2006).

### 2.5. Statistical analysis

Regional mean values of CBF, $rCMR_{Glu}$ and DVR were extracted from each ROI in each subject, which were tested for normality using the Shapiro-Wilk W test. According to the results of normality test, the correlations between regional mean rCBF and $rCMR_{Glu}$, absCBF and DVR, and $rCMR_{Glu}$ and DVR were calculated across subjects using Pearson or Spearman's correlation coefficients. Furthermore, the associations of the mean DVR in grey matter, which was treated as the global amyloid deposition, with voxel-level absCBF and $rCMR_{Glu}$ were also explored using a univariate regression analysis by SPM, respectively. The statistical maps were thresholded at a significance of $p < 0.001$ uncorrected with a cluster level threshold of 200 voxels. Voxel-by-voxel and cross-subject correlations were calculated between rCBF and R1 in each ROI using Pearson's correlation and Spearman's correlation, respectively. For ROI-wise correlation analysis, statistical significance was defined as $p < 0.05$ (2 tailed) uncorrected. Family wise correction of multiple comparisons was further performed in voxelwise analysis.

The age of symptom onset and dementia diagnosis tends to be fairly consistent within ADAD families and within persons with the same mutation (Ryman et al., 2014). Accordingly, one can estimate the number of years to clinically diagnosable dementia ("adjusted age") based on the age of dementia diagnosis in each subject's affected parent. Both linear and quadratic models were considered to model each imaging biomarker as a function of adjusted age to study the pathologic changes in Alzheimer's disease in mutation carriers for each AD-related ROI.

## 3. Results

The demographic characteristics of the research participants are listed in Table 1. There were 22 mutation-carriers and 9 non-carriers in total. The mutation carriers and non-carriers did not differ significantly in their age, sex, adjusted age, cognitive status, or proportion who were carriers of the APOE ε4 allele. Twenty-one (16 mutation-carriers) out of the total 31 subjects underwent complete assessments with ASL MRI, FDG PET and PiB PET scans, which were used for the analysis of intermodality comparisons. No significance was detected between the participants with and without completing imaging scans in their age, adjusted age, cognitive status and proportion of APOE ε4 carriers, except gender (Table S1).

### 3.1. Spatial patterns of cerebral blood flow, metabolism, and amyloid-β deposition

Normalized rCBF, $rCMR_{Glu}$ and DVR maps of the entire brain were averaged across subjects to compare their spatial patterns. As displayed in Fig. 1a–c, the mean rCBF and $rCMR_{Glu}$ maps show highly consistent spatial patterns with high contrast between grey and white matter, whereas PiB DVR shows a weaker contrast between cortical grey and white matter and a higher intensity in basal ganglia and thalamus. To further demonstrate the spatial similarity and difference between the CBF map and the $CMR_{Glu}$ and DVR maps, voxel-wise correlations between the mean rCBF and $rCMR_{Glu}$ and between the mean absCBF and DVR were performed in 9 CE-associated anatomical ROIs by calculating Pearson correlation coefficients. Scatter plots between the mean rCBF and $rCMR_{Glu}$, and between the mean absCBF and DVR in the 9 ROIs are shown in Fig. S1. Significantly positive correlations between rCBF and $rCMR_{Glu}$ were observed in all the ROIs with an overall mean correlation coefficient of $r = 0.57 \pm 0.16$. A reduced voxel-wise correlation ($r = 0.28 \pm 0.29$) was obtained between absCBF and DVR.

**Table 1**
The characteristics of the research cohort.

| Characteristics | ADAD mutation carriers ($N = 23$) | Non-carriers ($N = 8$) | $P$ value |
|---|---|---|---|
| Sex (F/M) | 16/7 | 3/5 | 0.12 |
| Age (range), yr | 41 ± 13 (19–64) | 32 ± 11 (22–56) | 0.09 |
| Adjusted age (range), yr | −10 ± 8 (−28–5) | −17 ± 10 (−27∼−1) | 0.09 |
| CDR > 0, no. | 12 | 4* | 0.48 |
| ApoE4 carriers, no. | 4 | 2 | 0.65 |
| Mutation type, no. | PS:19; APP:4 | | |

CDR: Cognitive Dementia Rating Score. CDR = 0 indicates no cognitive decline. CDR > 0 indicates cognitive decline.

* 4 non-carriers were blindly found to have CDR scores of 0.5 representing questionable cognitive impairment unrelated to early-onset AD.

### 3.2. Regional associations of cerebral blood flow, metabolism, and amyloid-β deposition

To study the coupling between CBF and metabolism in ADAD, regional correlations between the mean rCBF and mean $rCMR_{Glc}$ were calculated across the 21 subjects in the 9 AD-associated anatomical ROIs separately. The scatter plots of rCBF vs. $rCMR_{Glc}$ in each ROI are shown in Fig. 2. A global correlation of 0.08 ± 0.21 was obtained between rCBF and $rCMR_{Glu}$ across subjects with considerable variability across 9 ROIs. Specifically, positive correlations were mostly found in cortical regions including frontal, occipital, parietal and temporal cortex, while negative correlations were seen in subcortical regions, including amygdala, hippocampus, and insula.

The regional associations of amyloid deposition with cerebral perfusion and metabolism were also studied by calculating Spearman's correlation coefficients in the 9 ROIs across subjects, as shown in Fig. 3a and b, respectively. Overall, inverse correlations were obtained between DVR with both absCBF ($r = -0.15 \pm 0.16$), and $rCMR_{Glc}$ ($r = -0.31 \pm 0.23$) across subjects. The stronger regional correlation was seen in insula ($r = -0.35$) and cortical regions including temporal ($r = -0.31$) and frontal ($r = -0.32$) lobes with the lowest correlation seen in hippocampus ($r = -0.001$) for the cross-subject correlation of DVR and absCBF. The higher inverse correlation between DVR and $rCMR_{Glu}$ was seen in insula ($r = -0.56$) and cortical regions such as frontal ($r = -0.46$), occipital ($r = -0.46$) and parietal ($r = -0.47$) lobes with the lowest correlation seen in amygdala ($r = -0.03$).

### 3.3. Effects of global amyloid deposition on cerebral blood flow and cerebral metabolism

From the voxel-level regression analysis, we found regional CBF decreased in Frontal Mid L, Temporal Sup L, Temporal Mid&Sup R, and Parietal Inf L (Fig. 4) as the mean PiB DVR in grey matter increased. The findings remained significant after controlling for age, although the size

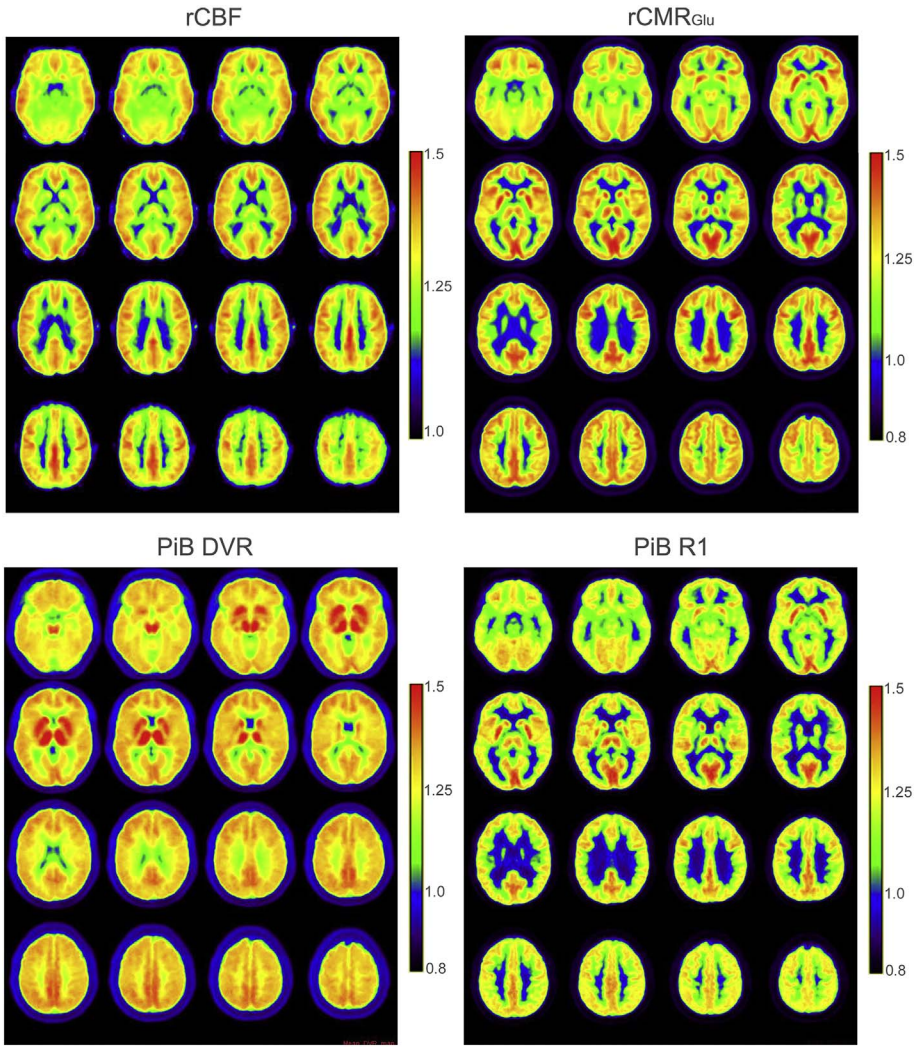


**Fig. 1.** The averaged rCBF, $rCMR_{Glu}$, PiB DVR and R1 maps across subjects. All the mean images were normalized to a MNI Collin template.

of the clusters was reduced. Significant inverse correlation was observed between the mean DVR in grey matter and the extracted CBF from each of the clusters (Fig. 4). The voxel-level regression analysis between $rCMR_{Glu}$ and global DVR suggested that regional metabolism decreased in Frontal Sup L&Mid R & Inf R, Temporal Sup R&L, Parietal Inf R, and Precentral L as the global amyloid deposition increased (Fig. 5). When correcting for the age effect, we still observed similar results. No regions with significant positive correlations between global DVR and $rCMR_{Glu}$ or rCBF were detected.

### 3.4. Trajectories of cerebral blood flow, cerebral metabolism, and amyloid deposition in ADAD mutation carriers in AD development

Since we focused on the trajectory of each individual biomarker, all the data available of each single modality from all the ADAD mutation carriers were included in the cross-sectional analysis to enlarge the sample size. Fig. 6 shows measures of cerebral blood flow, metabolism, and amyloid deposition as a function of adjusted age in ROIs relevant to AD processes. The cross-sectional plots show significant decline of CBF in cortical ROIs, including frontal, occipital, parietal and temporal lobes with adjusted age, as shown in Fig. 6a. A trend of decrease of CBF was also seen in precuneus. No significant change in CBF was found in hippocampus. For metabolism, only frontal cortex and several subcortical regions showed significant $rCMR_{Glu}$ decline. Similarly, the hippocampus did not show significant changes in glucose metabolism (Fig. 6b). For amyloid deposition, cortical ROIs including frontal, occipital, parietal, and temporal lobes showed increasing amyloid deposition as their age approaches the age of dementia diagnosis, but not in hippocampus (Fig. 6c). Significant increase of amyloid deposition was also found in precuneus.

### 3.5. Comparison of cerebral perfusion measured using ASL and PiB-PET

R1 derived from dynamic PiB PET data is related to tracer delivery, which reflects regional brain perfusion. As shown in Fig. 1d, the mean R1 map demonstrates a distinct contrast between grey and white matter that is highly consistent with the spatial pattern of ASL-CBF shown in Fig. 1a. Furthermore, a strong positive correlation between mean rCBF and R1 was obtained across voxels in each ROI with an overall mean correlation coefficient $r = 0.57 \pm 0.16$, as shown in Fig. 7a. The highest correlation was seen for caudate ($r = 0.74$) with the lowest correlation seen in hippocampus ($r = 0.29$). Intermediate positive correlations were also seen between regional rCBF and R1 across subjects (Fig. 7b), resulting in a mean correlation coefficient of $0.20 \pm 0.20$ with the highest correlation in parietal cortex ($r = 0.50$) and lowest correlation in insula ($r = -0.002$).

## 4. Discussion

### 4.1. ADAD as a model for multi-modality imaging studies in AD

The relationship among cerebral perfusion, metabolism, and

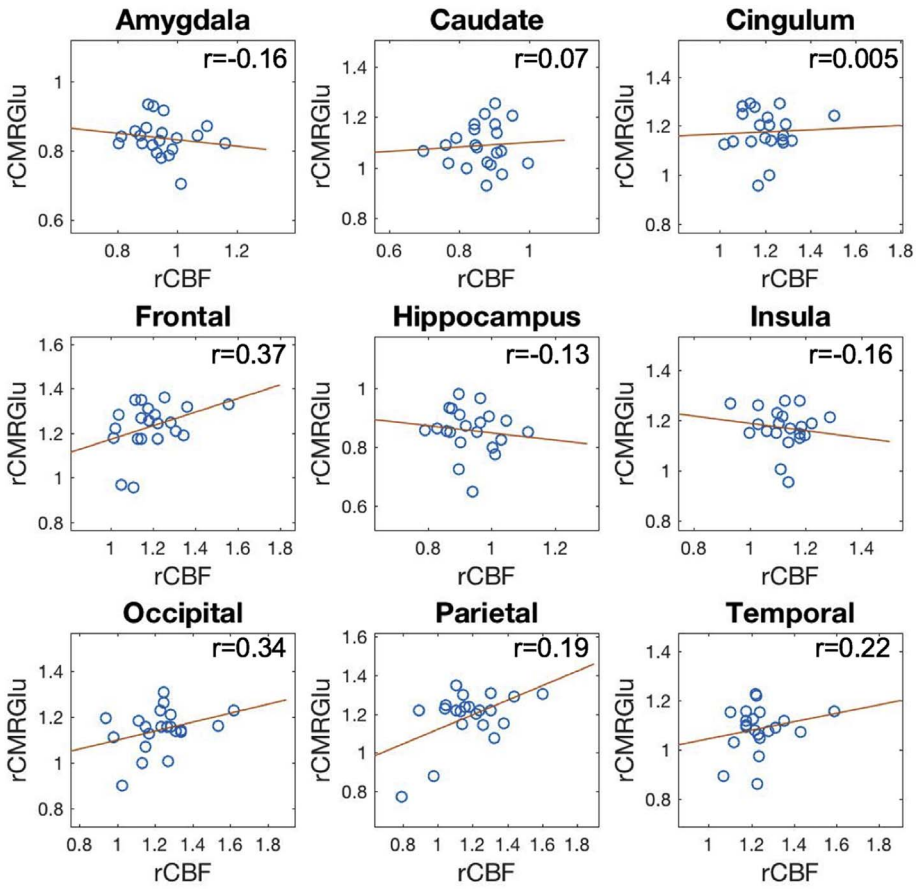


**Fig. 2.** Regional correlation between rCBF and $rCMR_{Glu}$ across 21 subjects in 9 anatomical ROIs relevant to AD. Spearman's correlation coefficients was calculated in caudate, cingulum, and parietal cortex, and Pearson's correlation was applied in the other ROIs.

amyloid deposition in people at risk for ADAD was investigated in this study. To our knowledge, this is the first study to compare pCASL MRI with both PiB PET and FDG PET in an ADAD cohort. Compared to late-onset AD, ADAD shows several advantages for investigating the association of cerebral perfusion with other biomarkers. In late-onset AD, abnormal CBF may be attributed to the presence of cerebrovascular disease rather than, or in addition to AD pathology (Dai et al., 2008), whereas persons at-risk for ADAD are younger and generally free of significant cerebrovascular disease and therefore provide the opportunity to measure CBF changes specific to AD pathophysiology. In our

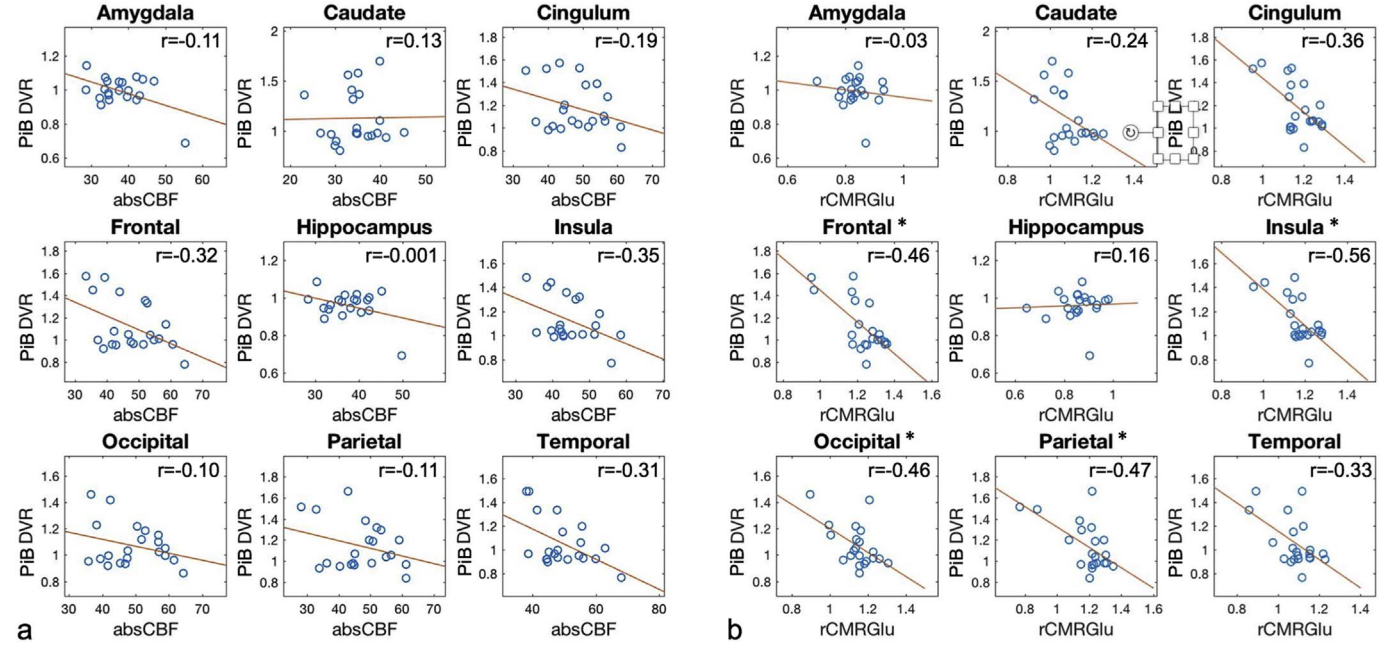


**Fig. 3.** Regional correlation between CBF vs. PiB DVR (a), and $rCMR_{Glu}$ vs. PiB DVR (b) across 21 subjects in 9 anatomical ROIs relevant to AD. (* indicates statistically significant correlation $p < 0.05$ uncorrected).

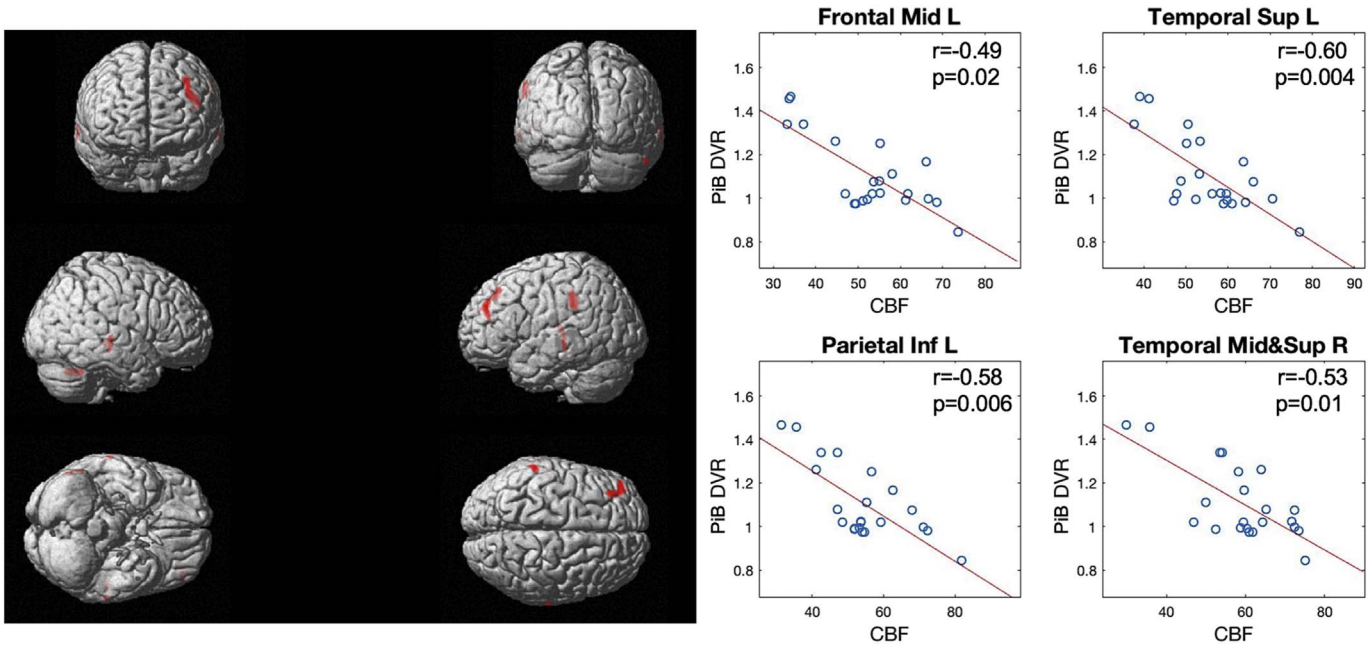


**Fig. 4.** The whole brain voxel-wise correlation of CBF maps with global PiB-PET DVR values that was calculated by the mean DVR values in grey matter. The significance level was $p < 0.001$ (uncorrected) with a cluster level of 200 voxels. The red regions represent the significantly inverse correlation of CBF with global DVR. The mean absolute CBF values were extracted from the detected significant regions, and the scatter plots between CBF from the hot regions and global DVR are shown on the right side. Adjusted $p$ values are listed in the scatter plots.

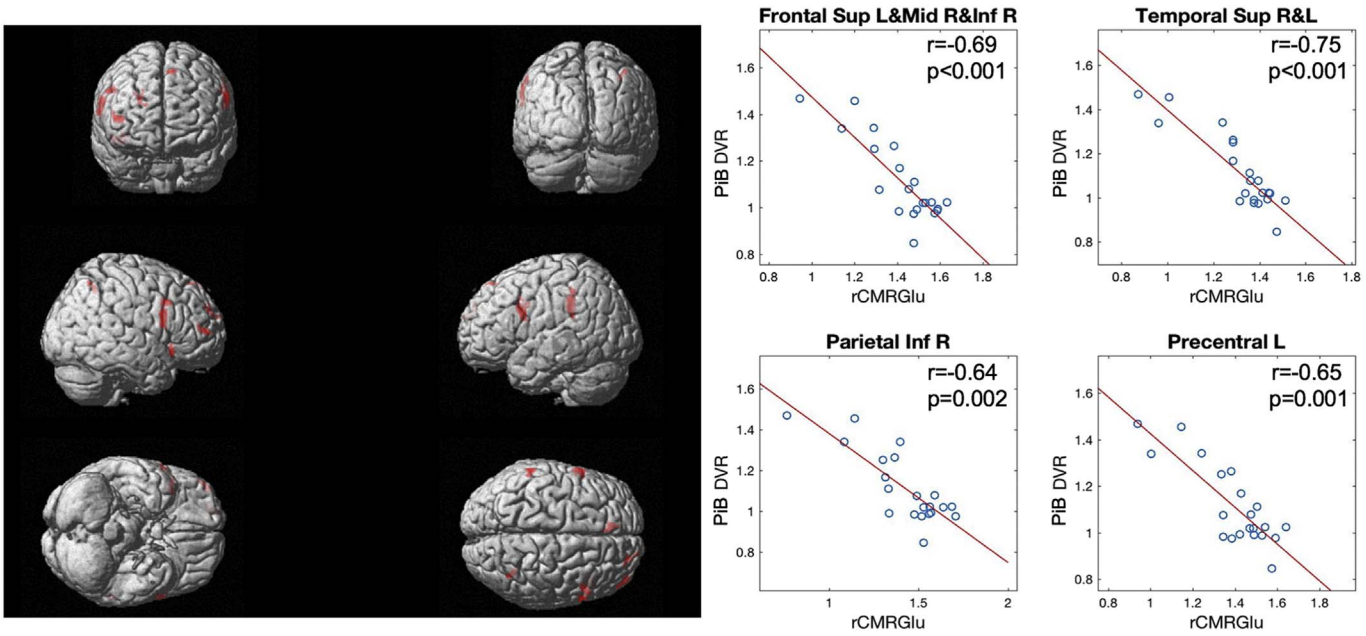


**Fig. 5.** The whole brain voxel-wise correlation of $rCMR_{Glu}$ maps with global PiB-PET DVR values calculated by the mean DVR values in grey matter. The significant level was $p < 0.001$ (uncorrected) with cluster level of 200 voxels. The red regions represent the significant regions where the $rCMR_{Glu}$ decreased with amyloid deposition. The mean $rCMR_{Glu}$ values were extracted from the detected significant regions, and the scatter plots between the mean $rCMR_{Glu}$ from the hot regions and global DVR are shown on the right side. Adjusted p values are listed in the scatter plots.

study, a similar spatial pattern with high contrast between grey and white matter was observed from rCBF and $rCMR_{Glu}$ maps, while DVR map exhibited a weaker contrast between grey and white matter with higher intensity in subcortical regions. Regional variability was found between rCBF and $rCMR_{Glu}$ across subject. Both absCBF and $rCMR_{Glu}$ show inverse associations with regional and global amyloid deposition across subjects, suggesting reduced regional cerebral perfusion and metabolism are related to increased amyloid deposition.

### 4.2. Relationship between regional CBF and $CMR_{Glu}$

Cerebral perfusion is generally thought to be closely related to metabolism. The association between cerebral perfusion and glucose metabolism has been investigated in normal populations, which shows an overall good correlation between CBF measured by ASL MRI and $CMR_{Glu}$ measured by FDG PET (Cha et al., 2013). It is generally believed that AD development is accompanied by a reduction of neuronal function in specific brain regions, manifested as regional reduction in metabolism and cerebral blood flow. Specific spatial patterns of hypo-

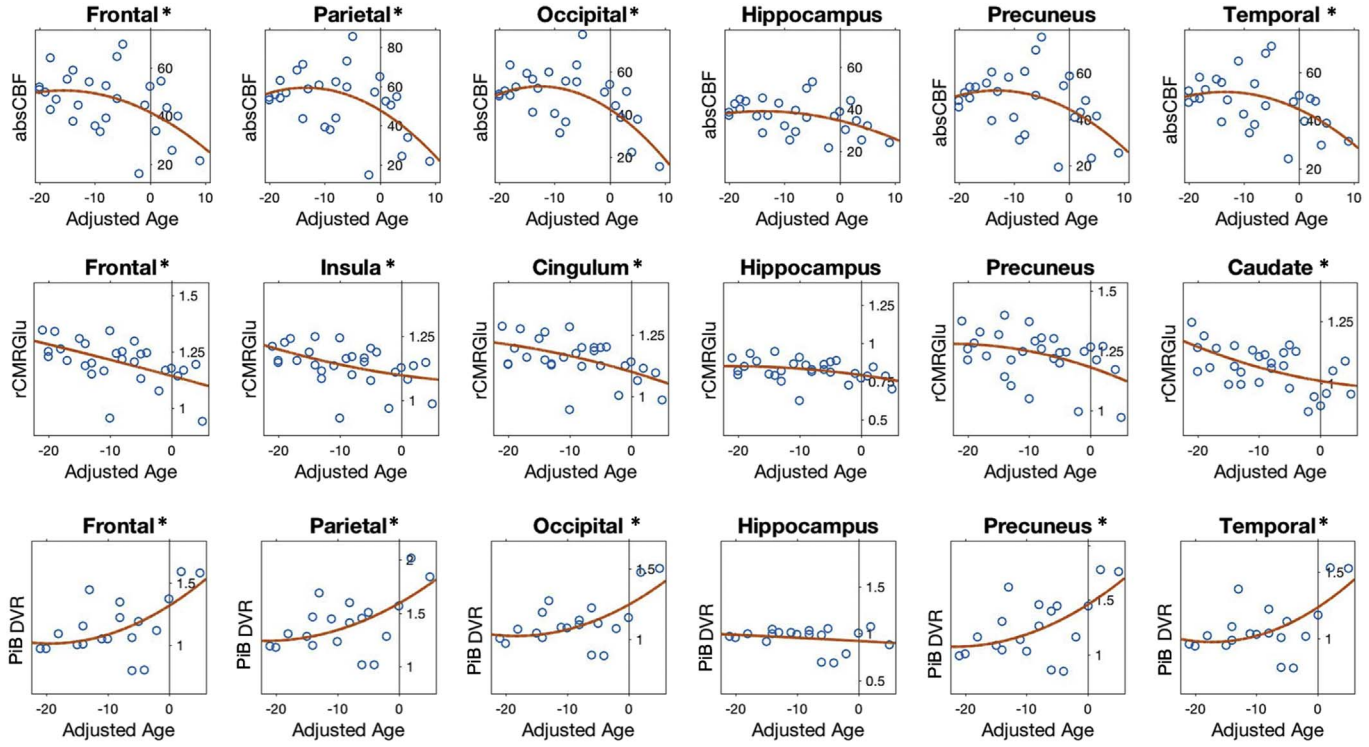


**Fig. 6.** The courses of regional CBF, $rCMR_{Glu}$, and PiB DVR as a function of the estimated year to dementia diagnosis (adjusted age) in ROIs using quadratic fitting model from mutation carriers. Only the regions with significant change with adjusted age as well as amygdala and precuneus were shown in the figure. Statistical Significance was defined as $p < 0.05$*.

metabolism and hypo-perfusion have been reported in AD patients (Alexander et al., 2002; Mosconi et al., 2009; Alsop et al., 2010; Z Wang et al., 2013a). In this study, we found a similar spatial pattern of cerebral perfusion and metabolism in ADAD subjects (Fig. 1a&b). However, a considerable variability of the regional correlation was observed between cerebral perfusion and metabolism across subjects (Fig. 2). Especially, inverse correlations were found in subcortical regions. The regional discrepancies between $rCMR_{Glu}$ and rCBF in people at risk for ADAD could be attributed to true perfusion-metabolism mismatch as a result of neurovascular decoupling during the development of AD, which is characterized by cerebrovascular pathology. Uncoupling between between $rCMR_{Glu}$ and rCBF in subcortical regions has been observed under pathological conditions, such as global ischemia of brain (Ueki et al., 1988). In this study, the observed decoupling between $rCMR_{Glu}$ and rCBF in subcortical regions may be directly involved in early AD pathology especially for persons at risk for AD at young age. On the other hand, the regional difference between $rCMR_{Glu}$ and rCBF could be caused by specific characteristics of each imaging modality

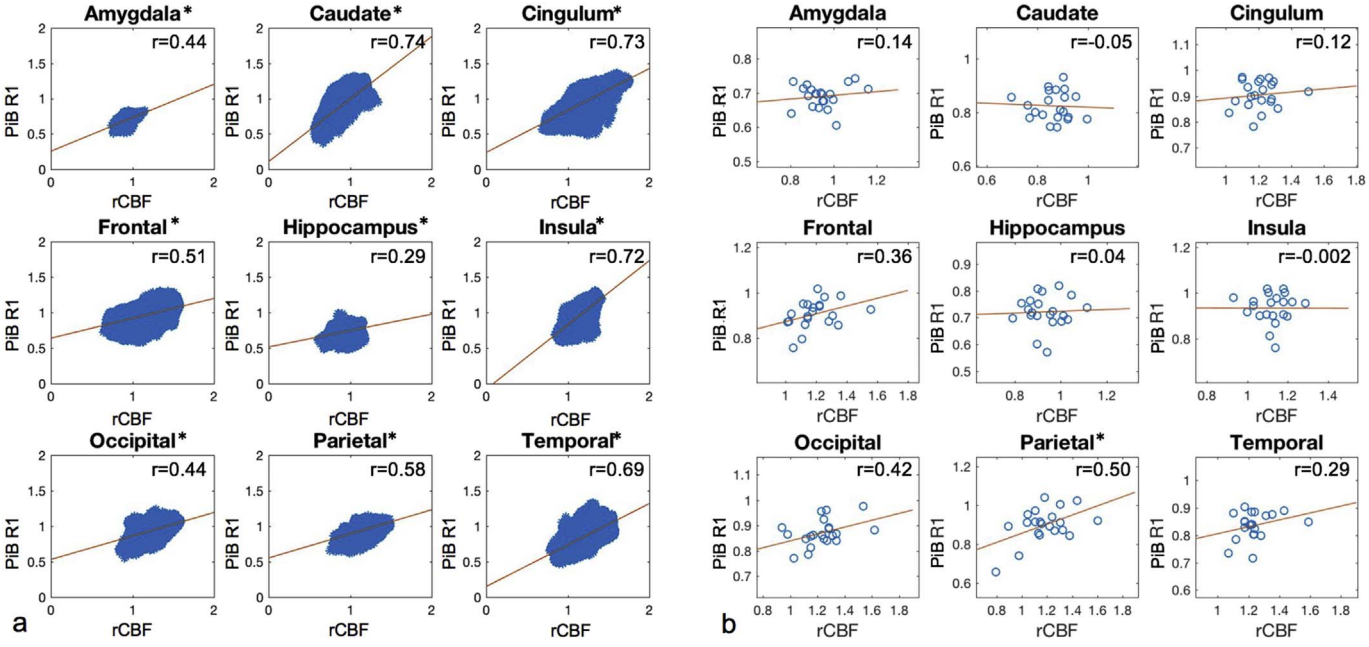


**Fig. 7.** The regional correlation between mean rCBF and PiB R1 was shown on a voxel-by-voxel basis (a) and across subject (b) in each AD associated ROI. (* indicates statistically significant correlation $p < 0.05$ with (a) and without (b) family wise correction).

(Cha et al., 2013).

### 4.3. Amyloid Deposition is associated with decrease in CBF and $rCMR_{Glu}$

According to the amyloid cascade hypothesis (Hardy & Higgins, 1992), the accumulation of amyloid plaques is a central event in the pathogenesis of AD. Reduction in cerebral perfusion and metabolism are also early events in AD pathogenesis (Murray et al., 2011). The alteration of cerebral perfusion associated with cerebral amyloid in ADAD was previously studied by McDade et al. (2014), which was focused on the voxel-level correlation of CBF map with global amyloid deposition. By contrast, the present study primarily investigated the associations between molecular, neuronal, and vascular biomarkers of AD from AD-relevant anatomical ROIs. A negative cross-subject correlation of DVR with both CBF and $rCMR_{Glu}$ was observed in each ROI, which suggests that brain regions with high amyloid deposition are associated with regional hypo-perfusion and hypo-metabolism. We also performed voxel-wise regression analysis, and found that hypo-perfusion and hypo-metabolism in regions of frontal, parietal and temporal cortex were significantly associated with global amyloid deposition (Figs. 4 and 5), which is in good agreement with previous findings (McDade et al., 2014). According to the vascular hypothesis in AD (Zlokovic, 2011), the inverse association between amyloid deposition and cerebral perfusion suggests the cerebral vascular dysfunction may be highly associated with amyloid pathology. However, a causal relationship between hypoperfusion and amyloid deposition cannot be concluded based on cross-sectional analyses such as these.

### 4.4. Evolution of regional CBF, $CMR_{Glu}$ and Amyloid Deposition with ADAD progression

Compared to late-onset AD, ADAD offers a unique advantage for studying the pathologic processes and disease progression of AD. Making use of the estimated years to dementia diagnosis helps define the stages of AD pathology. In this study, the courses of cerebral perfusion, metabolism, and amyloid deposition as a function of this adjusted age were studied in the 9 ROIs. Even with the relative small sample size, we were able to obtain similar findings as those reported in late-onset AD. Specifically, we found that ADAD mutation carriers presented increased amyloid deposition and decreased glucose metabolism and cerebral blood flow as they approached the age of dementia diagnosis. To confirm our findings, both linear and non-linear fitting models were considered in the cross-sectional plots, which showed very consistent results (Fig. 6 and Fig. S2). The significant decrease of CBF was mainly located in cortical regions, whereas significant decrease of glucose metabolism was shown in subcortical regions. This may also account for the variability of regional correlations between CBF and $CMR_{Glu}$. Such decoupling of regional CBF and metabolism years before dementia onset might provide important diagnostic and prognostic information. From the time courses of DVR, we found mutation carriers showed a rapid increase of amyloid deposition in most ROIs except for hippocampus before symptom onset, which is consistent with the findings from previous studies (Benzinger et al., 2013). The similar but inverse curves between CBF and DVR trajectories further suggest that the change of CBF may be closely associated with amyloid deposition, indicating that pCASL MRI may offer a sensitive biomarker for the early detection of AD pathology.

### 4.5. Relationship between ASL CBF and R1 of PiB PET

In this study, pCASL MRI was used for the measurement of cerebral perfusion. Previous studies have demonstrated that ASL shows great promise for the diagnosis, and early detection of neurodegenerative diseases (Binnewijzend et al., 2016; Alsop et al., 2010; Z Wang et al., 2013a; Dai et al., 2009). Because of its easy implementation and non-invasive nature, ASL is now part of routine clinical MRI protocols. In our study, pseudo-continuous ASL (pCASL) with 3D background-suppressed single-shot GRASE was used for ASL data collection. Compared to previous studies, background-suppressed pCASL-GRASE offers improved signal-to-noise ratio and higher reproducibility, thereby providing a more reliable imaging biomarker (Kilroy et al., 2014). We further systematically compared pCASL with R1 at both voxel-wise and cross-subject levels. R1 was calculated from PiB PET using SUVR model and has been considered as a proxy of relative CBF. As expected, similar spatial patterns and significant voxel-wise correlations between rCBF and R1 were observed in the 9 ROIs, since both parameters reflect brain perfusion. An intermediate positive regional correlation between rCBF and R1 was also obtained across subjects. Our findings support that pCASL MRI is a promising non-invasive imaging technique that has the potential to serve as a clinical tool for the measurement of CBF in AD.

### 4.6. Potential confounding factors and limitations

There were some potential confounding factors involved in our analyses. First of all, partial volume effects between grey and white matter may contribute to the correlation among CBF, $rCMR_{Glu}$ and DVR. To minimize such problem, a high grey matter threshold was applied to CBF, R1 and DVR images and only the data from voxels that exceeded the grey matter threshold were used for data analysis. Furthermore, this study focused on the regional association of multiple imaging modalities across subjects, therefore, the variation induced by the correction of partial volume in the correlation analysis is unlikely to significantly affect the overall findings, which has been confirmed in previous studies. Secondly, a previous study reported there was amyloid deposition in cerebellum in ADAD (Mann et al., 2001). Thus, the cerebellar grey matter used as a reference region for the amyloid quantification may reduce the effects of amyloid deposition across subjects. Nevertheless, significant increases of amyloid accumulation with adjusted age were still observed in the cross-sectional plots. Thirdly, we also considered the effect of brain atrophy on the measures of each imaging biomarkers along the cascade of AD pathologic progression. The regional values of each biomarker were divided by Jacobian determinants calculated from the T1 structural images of each participant to account for the potential effect of structural variations. Similar biomarker courses persisted after Jacobian determinant correction, though with reduced significance (Fig. S3&4).

Our study has several limitations. First of all, a single PLD of 1500 ms was applied in ASL acquisitions, which at the time of the study was appropriate but may be inferior to a PLD of 1800–2000 ms as recommended for neurodegenerative studies in the recently published ASL white paper (Alsop et al., 2015). Moreover, arterial transit time may vary among subjects, especially for AD patients, causing potential inaccuracy of CBF measurement. Multi-delay ASL (Wang et al., 2013b) could be an alternative option for CBF measurement in AD. Secondly, there were relatively few non-mutation carriers, so we were not able to sensitively compare the trajectories of the three biomarkers during ADAD pathologic processes between mutation and non-mutation carriers. Thirdly, this is a cross-sectional study with relatively small sample size; the causal relationship between the three biomarkers along the ADAD development can't be fully studied. To demonstrate the temporal and causal relationship of cerebral perfusion with metabolism and amyloid deposition, additional longitudinal studies with adequate sample size will be required in the future.

## 5. Conclusion

The regional associations among cerebral perfusion, metabolism, and amyloid deposition in a cohort of ADAD-related subjects were investigated. Cerebral blood flow measured by pCASL MRI shows similar spatial pattern with metabolism measured by FDG-PET across subjects. However, there was considerable variability across brain regions, wherein the negative correlations may indicate neurovascular

decoupling and may be related to AD pathology. Both cerebral perfusion and metabolism showed inverse correlation with regional and global amyloid deposition. This finding suggests high amyloid deposition is associated with hypo-perfusion and/or hypo-metabolism, which is in accordance with the vascular hypothesis of AD. This study suggests that ASL, FDG-PET and PiB-PET may provide complementary information for understanding the pathophysiology and progression of AD.

## Acknowledgements

This study is supported by NIH grants R21TW009787, UH2NS100614, U19 AG032438, 1UL1-RR033176, 1K25AG056594, AHA grant 16SDG29630013, Alzheimer's Disease Research Center Grants P50 AG-016570, P50 AG-005142, U01 AG-051218, M01-RR00865, the Easton Consortium for Alzheimer's Disease Drug Discovery and Biomarker Development.

## Disclosures/conflict of interest

The authors declare no conflict of interest.

## Appendix A. Supplementary data

Supplementary data to this article can be found online at https://doi.org/10.1016/j.nicl.2017.12.003.

## References

Alexander, G.E., Chen, K., Pietrini, P., Rapoport, S.I., Reiman, E.M., 2002. Longitudinal PET evaluation of cerebral metabolic decline in dementia: a potential outcome measure in Alzheimer's disease treatment studies. Am. J. Psychiatry 159, 738–745.
Alsop, D.C., Detre, J.A., Grossman, M., 2000. Assessment of cerebral blood flow in Alzheimer's disease by spin-labeled magnetic resonance imaging. Ann. Neurol. 47, 93–100.
Alsop, D.C., Dai, W., Grossman, M., Detre, J.A., 2010. Arterial spin labeling blood flow MRI: its role in the early characterization of Alzheimer's disease. J. Alzheimers Dis. 20, 871–880.
Alsop, D.C., Detre, J.A., Golay, X., et al., 2015. Recommended implementation of arterial spin-labeled perfusion MRI for clinical applications: a consensus of the ISMRM perfusion study group and the European consortium for ASL in dementia. Magn. Reson. Med. 73, 102–116.
Avants, B., Duda, J.T., Kim, J., et al., 2008. Multivariate analysis of structural and diffusion imaging in traumatic brain injury. Acad. Radiol. 15, 1360–1375.
Bateman, R.J., Aisen, P.S., De Strooper, B., et al., 2011. Autosomal-dominant Alzheimer's disease: a review and proposal for the prevention of Alzheimer's disease. Alzheimers Res. Ther. 3, 1.
Bateman, R.J., Xiong, C., Benzinger, T.L., et al., 2012. Clinical and biomarker changes in dominantly inherited Alzheimer's disease. N. Engl. J. Med. 367, 795–804.
Benzinger, T.L., Blazey, T., Jack Jr., C.R., et al., 2013. Regional variability of imaging biomarkers in autosomal dominant Alzheimer's disease. Proc. Natl. Acad. Sci. U. S. A. 110, E4502–4509.
Berti, V., Osorio, R.S., Mosconi, L., Li, Y., De Santi, S., de Leon, M.J., 2010. Early detection of Alzheimer's disease with PET imaging. Neurodegener. Dis. 7, 131–135.
Binnewijzend, M.A., Kuijer, J.P., Benedictus, M.R., et al., 2013. Cerebral blood flow measured with 3D pseudocontinuous arterial spin-labeling MR imaging in Alzheimer disease and mild cognitive impairment: a marker for disease severity. Radiology 267, 221–230.
Binnewijzend, M.A., Benedictus, M.R., Kuijer, J.P., et al., 2016. Cerebral perfusion in the predementia stages of Alzheimer's disease. Eur. Radiol. 26, 506–514.
Cha, Y.H., Jog, M.A., Kim, Y.C., Chakrapani, S., Kraman, S.M., Wang, D.J., 2013. Regional correlation between resting state FDG PET and pCASL perfusion MRI. J. Cereb. Blood Flow Metab. 33, 1909–1914.
Chen, Y., Wolk, D.A., Reddin, J.S., et al., 2011. Voxel-level comparison of arterial spin-labeled perfusion MRI and FDG-PET in Alzheimer disease. Neurology 77, 1977–1985.
Dai, W., Lopez, O.L., Carmichael, O.T., Becker, J.T., Kuller, L.H., Gach, H.M., 2008. Abnormal regional cerebral blood flow in cognitively normal elderly subjects with hypertension. Stroke 39, 349–354.
Dai, W., Lopez, O.L., Carmichael, O.T., Becker, J.T., Kuller, L.H., Gach, H.M., 2009. Mild cognitive impairment and alzheimer disease: patterns of altered cerebral blood flow at MR imaging. Radiology 250, 856–866.
Detre, J.A., Wang, J., Wang, Z., Rao, H., 2009. Arterial spin-labeled perfusion MRI in basic and clinical neuroscience. Curr. Opin. Neurol. 22, 348–355.
Dickstein, D.L., Walsh, J., Brautigam, H., Stockton Jr., S.D., Gandy, S., Hof, P.R., 2010. Role of vascular risk factors and vascular dysfunction in Alzheimer's disease. Mt Sinai J. Med. 77, 82–102.
Du, A.T., Jahng, G.H., Hayasaka, S., et al., 2006. Hypoperfusion in frontotemporal dementia and Alzheimer disease by arterial spin labeling MRI. Neurology 67, 1215–1220.
Dubois, B., Hampel, H., Feldman, H.H., et al., 2016. Preclinical Alzheimer's disease: definition, natural history, and diagnostic criteria. Alzheimers Dement. 12, 292–323.
Ewers, M., Sperling, R.A., Klunk, W.E., Weiner, M.W., Hampel, H., 2011. Neuroimaging markers for the prediction and early diagnosis of Alzheimer's disease dementia. Trends Neurosci. 34, 430–442.
Fennema-Notestine, C., McEvoy, L.K., Hagler Jr., D.J., Jacobson, M.W., Dale, A.M., 2009. The Alzheimer's disease neuroimaging I. Structural neuroimaging in the detection and prognosis of pre-clinical and early AD. Behav. Neurol. 21, 3–12.
Forsberg, A., Engler, H., Almkvist, O., et al., 2008. PET imaging of amyloid deposition in patients with mild cognitive impairment. Neurobiol. Aging 29, 1456–1465.
Frisoni, G.B., 2012. Alzheimer disease: biomarker trajectories across stages of Alzheimer disease. Nat. Rev. Neurol. 8, 299–300.
Frisoni, G.B., Fox, N.C., Jack Jr., C.R., Scheltens, P., Thompson, P.M., 2010. The clinical use of structural MRI in Alzheimer disease. Nat. Rev. Neurol. 6, 67–77.
Hardy, J.A., Higgins, G.A., 1992. Alzheimer's disease: the amyloid cascade hypothesis. Science 256, 184–185.
Hays, C.C., Zlatar, Z.Z., Wierenga, C.E., 2016. The utility of cerebral blood flow as a biomarker of preclinical Alzheimer's disease. Cell. Mol. Neurobiol. 36, 167–179.
Johnson, N.A., Jahng, G.H., Weiner, M.W., et al., 2005. Pattern of cerebral hypoperfusion in Alzheimer disease and mild cognitive impairment measured with arterial spin-labeling MR imaging: initial experience. Radiology 234, 851–859.
Kilroy, E., Apostolova, L., Liu, C., Yan, L., Ringman, J., Wang, D.J., 2014. Reliability of two-dimensional and three-dimensional pseudo-continuous arterial spin labeling perfusion MRI in elderly populations: comparison with 15O-water positron emission tomography. J. Magn. Reson. Imaging 39, 931–939.
Klunk, W.E., Engler, H., Nordberg, A., et al., 2004. Imaging brain amyloid in Alzheimer's disease with Pittsburgh compound-B. Ann. Neurol. 55, 306–319.
Lammertsma, A.A., Hume, S.P., 1996. Simplified reference tissue model for PET receptor studies. NeuroImage 4, 153–158.
Loessner, A., Alavi, A., Lewandrowski, K.U., Mozley, D., Souder, E., Gur, R.E., 1995. Regional cerebral function determined by FDG-PET in healthy volunteers: normal patterns and changes with age. J. Nucl. Med. 36, 1141–1149.
Logan, J., 2000. Graphical analysis of PET data applied to reversible and irreversible tracers. Nucl. Med. Biol. 27, 661–670.
Mann, D.M., Pickering-Brown, S.M., Takeuchi, A., Iwatsubo, T., 2001. Members of the familial Alzheimer's disease pathology study G. Amyloid angiopathy and variability in amyloid beta deposition is determined by mutation position in presenilin-1-linked Alzheimer's disease. Am. J. Pathol. 158, 2165–2175.
Mattsson, N., Tosun, D., Insel, P.S., et al., 2014. Association of brain amyloid-beta with cerebral perfusion and structure in Alzheimer's disease and mild cognitive impairment. Brain 137, 1550–1561.
McDade, E., Kim, A., James, J., et al., 2014. Cerebral perfusion alterations and cerebral amyloid in autosomal dominant Alzheimer disease. Neurology 83, 710–717.
McDonald, C.R., McEvoy, L.K., Gharapetian, L., et al., 2009. Regional rates of neocortical atrophy from normal aging to early Alzheimer disease. Neurology 73, 457–465.
Mosconi, L., 2005. Brain glucose metabolism in the early and specific diagnosis of Alzheimer's disease. FDG-PET studies in MCI and AD. Eur. J. Nucl. Med. Mol. Imaging 32, 486–510.
Mosconi, L., Mistur, R., Switalski, R., et al., 2009. FDG-PET changes in brain glucose metabolism from normal cognition to pathologically verified Alzheimer's disease. Eur. J. Nucl. Med. Mol. Imaging 36, 811–822.
Mosconi, L., Berti, V., Glodzik, L., Pupi, A., De Santi, S., de Leon, M.J., 2010. Pre-clinical detection of Alzheimer's disease using FDG-PET, with or without amyloid imaging. J. Alzheimers Dis. 20, 843–854.
Murray, I.V., Proza, J.F., Sohrabji, F., Lawler, J.M., 2011. Vascular and metabolic dysfunction in Alzheimer's disease: a review. Exp. Biol. Med. (Maywood) 236, 772–782.
Reiman, E.M., Chen, K., Alexander, G.E., et al., 2004. Functional brain abnormalities in young adults at genetic risk for late-onset Alzheimer's dementia. Proc. Natl. Acad. Sci. U. S. A. 101, 284–289.
Ryman, D.C., Acosta-Baena, N., Aisen, P.S., et al., 2014. Symptom onset in autosomal dominant Alzheimer disease: a systematic review and meta-analysis. Neurology 83, 253–260.
Schindler, S.E., Fagan, A.M., 2015. Autosomal dominant Alzheimer disease: a unique resource to study CSF biomarker changes in preclinical AD. Front. Neurol. 6, 142.
Smailagic, N., Vacante, M., Hyde, C., Martin, S., Ukoumunne, O., Sachpekidis, C., 2015. (1)(8)F-FDG PET for the early diagnosis of Alzheimer's disease dementia and other dementias in people with mild cognitive impairment (MCI). Cochrane Database Syst. Rev. 1, CD010632.
Small, G.W., Kepe, V., Ercoli, L.M., et al., 2006. PET of brain amyloid and tau in mild cognitive impairment. N. Engl. J. Med. 355, 2652–2663.
Ueki, M., Linn, F., Hossmann, K.A., 1988. Functional activation of cerebral blood flow and metabolism before and after global ischemia of rat brain. J. Cereb. Blood Flow Metab. 8, 486–494.
Vemuri, P., Jack Jr., C.R., 2010. Role of structural MRI in Alzheimer's disease. Alzheimers Res. Ther. 2, 23.
Vlassenko, A.G., Benzinger, T.L., Morris, J.C., 2012. PET amyloid-beta imaging in preclinical Alzheimer's disease. Biochim. Biophys. Acta 1822, 370–379.
Wang, Z., Das, S.R., Xie, S.X., et al., 2013a. Arterial spin labeled MRI in prodromal Alzheimer's disease: a multi-site study. Neuroimage Clin. 2, 630–636.
Wang, D.J., Alger, J.R., Qiao, J.X., et al., 2013b. Multi-delay multi-parametric arterial spin-labeled perfusion MRI in acute ischemic stroke - comparison with dynamic susceptibility contrast enhanced perfusion imaging. Neuroimage Clin. 3, 1–7.
WT, Hu, Wang, Z., Lee, V.M., Trojanowski, J.Q., Detre, J.A., Grossman, M., 2010. Distinct cerebral perfusion patterns in FTLD and AD. Neurology 75, 881–888.

Ye, F.Q., Berman, K.F., Ellmore, T., et al., 2000. H(2)(15)O PET validation of steady-state arterial spin tagging cerebral blood flow measurements in humans. Magn. Reson. Med. 44, 450–456.
Ye, H., Wong, K.P., Wardak, M., et al., 2014. Automated movement correction for dynamic PET/CT images: evaluation with phantom and patient data. PLoS One 9, e103745.
Zhang, S., Smailagic, N., Hyde, C., et al., 2014a. (11)C-PIB-PET for the early diagnosis of Alzheimer's disease dementia and other dementias in people with mild cognitive impairment (MCI). Cochrane Database Syst. Rev. 7, CD010386.
Zhang, K., Herzog, H., Mauler, J., et al., 2014b. Comparison of cerebral blood flow acquired by simultaneous [15O]water positron emission tomography and arterial spin labeling magnetic resonance imaging. J. Cereb. Blood Flow Metab. 34, 1373–1380.
Zlokovic, B.V., 2011. Neurovascular pathways to neurodegeneration in Alzheimer's disease and other disorders. Nat. Rev. Neurosci. 12, 723–738.